Am J Transl Res 2025;17(8):6275-6290
www.ajtr.org /ISSN:1943-8141/AJTR0166281

Original Article

Three-dimensional finite element analysis of the influence of different stress modes in invisible aligners on anterior teeth retraction

Jing Xiong[1], Ying Zhang[1], Lei Liu[2]

[1]Department of Stomatology, Hanzhong Central Hospital, Hanzhong 723000, Shaanxi, China; [2]Medical Record Statistics Section, Hanzhong Central Hospital, Hanzhong 723000, Shaanxi, China

Received May 23, 2025; Accepted July 28, 2025; Epub August 15, 2025; Published August 30, 2025

Abstract: Objective: To investigate the effects of different stress application methods of invisible aligners on anterior tooth retraction using three-dimensional finite element analysis. Methods: An adult patient with maxillary protrusion undergoing orthodontic treatment with the extraction of the first premolars was selected for modeling. Five working conditions were simulated: ① Invisible aligner applying force for overall retraction of the maxillary anterior teeth; ② Invisible aligner combined with a micro - implant placed at the canine region's precise cutting site, applying a 1N force for overall anterior retraction; ③ Same as condition 2, with an additional 1 N force applied between the anchorage micro-implant near the maxillary central incisors and the aligner; ④ Invisible aligner applying a 1 N force at the canine region's precise cutting site for overall retraction; ⑤ Invisible aligner applying force combined with power ridge technology for root - controlled retraction of anterior teeth. Displacement and stress measurements-including displacement and stress at the coronal-radicular junction and periodontal ligament, as well as their components along the X (mesiodistal), Y (labiolingual), and Z (vertical) axes under different working conditions-were compared. Results: Total tooth displacements were similar across all conditions (range: 0.23197-0.23276 mm), with conditions ③ and ⑤ showing slightly lower displacement, though differences were not statistically significant. Stress at the coronal-radicular junction varied between 63.298-63.964 MPa, with conditions ② and ④ exhibiting slightly higher values. Condition ⑤ demonstrated a slight reduction in junction stress (63.703 MPa), attributed to root - control technology. Periodontal ligament stress showed a gradual increase from 0.41426 MPa (condition ①) to 0.41634 MPa (condition ⑤), representing a minimal overall change. Displacement was predominantly along the Y axis (approximately 0.205-0.206 mm), with smaller movements in the X (0.055-0.056 mm) and Z (0.095-0.096 mm) directions. Conclusion: All 5 working conditions produced comparable displacement outcomes, with condition ⑤ offering an advantage in reducing stress at the coronal-radicular junction, suggesting a benefit of root-controlled retraction in clinical application.

Keywords: Invisible aligner, anterior teeth retraction, stress mode, three-dimensional finite element, biomechanics

Introduction

With the development of artificial intelligence and digital technologies, orthodontic treatment techniques have undergone significant evolution. Invisible aligners are removable orthodontic appliances manufactured using computer - aided design and manufacturing combined with polymer thermoplastic materials. These aligners exert corrective forces through elastic deformation of the material to facilitate controlled tooth movement [1]. Compared with traditional fixed orthodontic appliances, invisible aligners offer distinct advantages, including superior aesthetics, enhanced comfort, ease of self-removal, and improved oral hygiene maintenance, all of which substantially increase patient compliance and overall treatment experience [2]. Driven by continuous progress in material science and computer technology, the efficacy of invisible orthodontic treatments is increasingly comparable to-and in some aspects surpasses-that of conventional fixed appliances, positioning them as the preferred choice for many patients. In the development process of invisible orthodontic technology, a

https://doi.org/10.62347/YGFV7405

comprehensive understanding of the underlying biomechanical mechanisms is crucial for enhancing treatment effects and ensuring patient safety. The finite element method, a mathematical and physical modeling technique, addresses this need by discretizing complex continuous structures into a finite number of elements. This process reduces an infinite-degree-of-freedom problem to a manageable finite-degree-of-freedom problem, enabling precise prediction of biomechanical behavior in complex models [3]. The three-dimensional finite element method has become an effective tool in stomatological research due to its high accuracy and non - invasive nature, and it is widely used in the biomechanical analysis of orthodontic treatments [4, 5]. While most existing studies focus on the biomechanics of traditional fixed orthodontic appliances, there remains a paucity of research addressing the stress distribution patterns of invisible aligners during the movement of teeth with low mutation abundance, especially regarding the combined application of micro-implant screws and dynamic ridge technology. This study hypothesizes that different stress application methods influence the displacement efficiency and biomechanical safety of anterior tooth retraction by changing the stress distribution within the tooth-periodontal ligament complex. Specifically, stress application strategies integrating micro-implant screws and dynamic ridge techniques may optimize mechanical force transmission. Therefore, this study employs three-dimensional finite element analysis method to deeply explore the effects of different stress application methods of invisible aligners on tooth movement and periodontal tissue stress distribution during anterior teeth retraction, providing a reliable biomechanical basis for the optimal design of clinical invisible orthodontic treatment plans.

Data and methods

Research subject

An adult patient undergoing orthodontic treatment for maxillary protrusion, with the extraction of the first premolar, was selected for this study. This patient exhibited no abnormalities in periodontal or dental tissues, no evident periodontal diseases, no prior orthodontic treatment, and no history of oral or maxillofacial trauma. After obtaining informed consent, the patient's maxilla and teeth were scanned using cone-beam computed tomography (CBCT) equipment (Beijing Langshi Instrument Co., LTD). During imaging, patient positioning was carefully standardized to ensure accuracy: the head was maintained in the natural midline position, with the orbital and auricular planes parallel to the ground. CBCT scans were acquired with a slice thickness of 0.125 mm, generating continuous tomographic images of the maxilla and teeth. The resulting data were stored in DICOM format to facilitate precise model reconstruction.

Model establishment

The collected CBCT image data in DICOM format were imported into the Mimics software for processing. Initially, the software's threshold segmentation function was employed to set appropriate gray value ranges based on the differential X-ray absorption characteristics of various tissues. For the hard tissues of the teeth, which exhibit relatively high gray values, upper and lower threshold limits were defined to segment the teeth from surrounding soft tissues and background, thereby generating an initial tooth mask. To extract the periodontal ligament, manual delineation was combined with auxiliary tools to gradually outline its contours and produce the periodontal ligament mask. Similarly, the maxilla was segmented by leveraging its gray-scale characteristics, and the three-dimensional contour information of the maxilla was extracted through operations such as threshold segmentation and region growth. Throughout the entire process, multiple views-including coronal, sagittal, and axial planes-were frequently reviewed to carefully inspect and refine the extracted structures, ensuring their integrity and accuracy. The finalized masks for the teeth, periodontal ligament and maxilla were then reconstructed into a three-dimensional reconstruction to generate corresponding three-dimensional models. Mimics was used for threshold segmentation and three-dimensional reconstruction, and Geomagic was used to optimize the surface quality of the models, followed by assembly of the components in Solidworks. Finally, a three-dimensional finite element model including the maxilla, teeth, periodontal ligament and invisible orthodontic appliance was constructed.

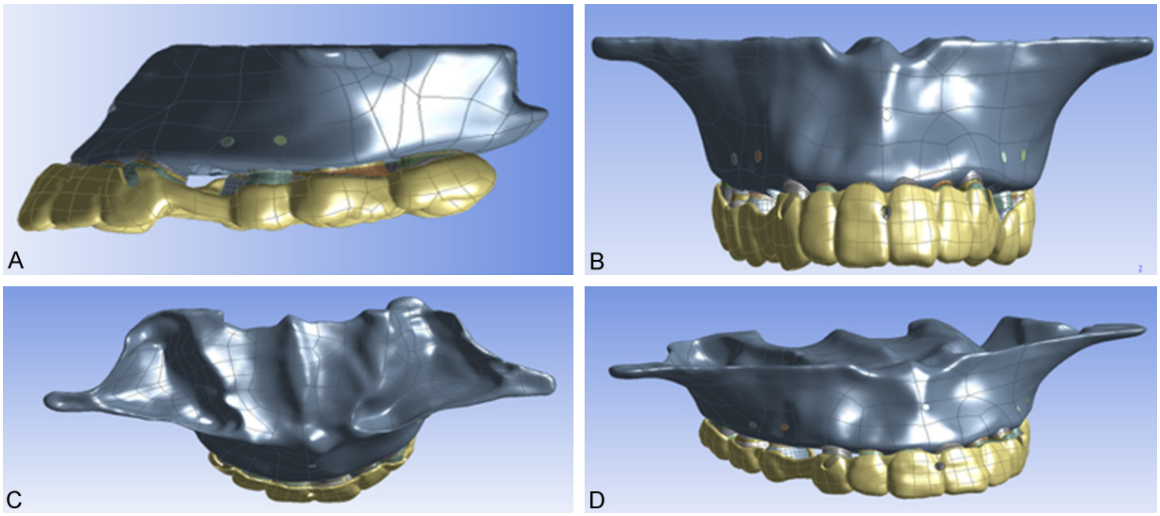

Figure 1. Three-dimensional tooth assembly model. A: View along the X-axis; B: View along the Y-axis; C: View along the Z-axis; D: Isometric view.

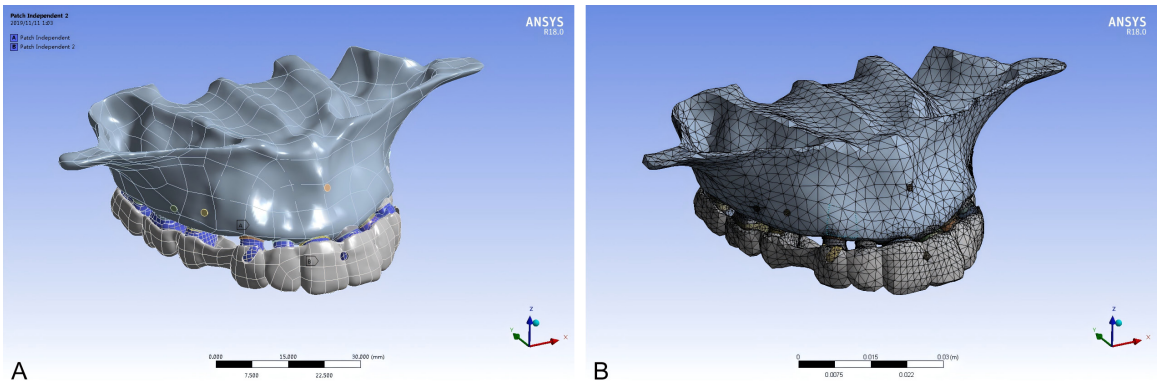

Figure 2. Finite element mesh of the established model.

Representative 3D views and XYZ iso-surfaces of the processed tooth assembly are shown in **Figure 1**.

Finite element mesh establishment

After assembly of the geometric model, it was imported into Hypermesh 2021 with a mesh size of 0.15 mm. Element quality was assessed through the element inspection instructions. To achieve an optimal balance between computational efficiency and accuracy, first-order tetrahedral elements were assigned to the teeth and associated components, while second-order tetrahedral elements were applied to the periodontal ligament and orthodontic appliances. The mesh models of each component were saved in INP format. Given the complexity of the dental assembly, tetrahedral meshes were adopted throughout. Validation showed that the accuracy of nodal tetrahedral meshes closely approximated that of hexahedral meshes. At the coronal-radicular junction, a mesh element size of 1 mm was applied, while default element sizes were used for other regions. The final mesh comprised 345,493 elements 83,606 nodes. A visualization of the mesh model is provided in **Figure 2**.

Measurement definition and material assignment

This study evaluated the initial tooth displacement and stress distribution within the periodontal ligament under orthodontic loading. All materials and tissues were modeled as ideal-

Table 1. Material properties and parameters definitions

Material	Young's modulus (MPa)	Poisson's ratio
Jawbone	1.38E+10	0.26
Corrector	5.28E+08	0.36
Dental crown	2E+09	0.30
Tooth body	2E+10	0.30
Periodontal ligament	6.8E+05	0.49
Planting nails	2.01E+11	0.33

ized isotropic, homogeneous and linearly elastic materials. The assigned material properties are shown in **Table 1**.

Working condition settings

Condition ① (A): Simulate overall retraction of the maxillary anterior teeth by applying force through the invisible orthodontic appliance, corresponding to a 0.25 mm uniform retraction according to the invisible orthodontic method. Condition ② (B): Simulate force application with the invisible orthodontic appliance combined with a 1 N force applied at the precise cutting site of the appliance at the canine cusp, located between the first molar and the second premolar, to retract the maxillary anterior teeth as a whole. Condition ③ (C): Simulate force application with the invisible orthodontic appliance combined with a micro-implant screw placed at the canine cusp (between the first molar and the second premolar) applying 1 N of force, plus an additional 1 N of force applied between the upper central incisors via the orthodontic appliance to assist overall anterior teeth retraction. Condition ④ (D): Simulate force application with the invisible orthodontic appliance combined with micro-implant screws placed at the proximal center of the second premolars and the incisors, applying a 1 N force at the precise cutting site of the appliance to achieve overall anterior teeth retraction. Condition ⑤ (E): Simulate force application with the invisible orthodontic appliance combined with power ridge for root-controlled anterior tooth retraction. A 1 N force is applied to retract the anterior teeth, while the root control force couples of 1 N each are applied respectively at the cervical labial side and the proximal lingual cutting edge (**Figure 3**).

Measurement and analysis indicators

(1) Stress distribution maps of teeth and periodontal ligament under different working conditions; (2) Displacement measurements under different working conditions, including: stress at the coronal-radicular junction, stress within the periodontal ligament, displacement of the coronal-radicular junction overall and along the X, Y, and Z directions, displacement of the periodontal ligament overall and along the X, Y, and Z directions.

Results

Cloud map of anterior tooth movement trends

Condition ①: The maximum overall deformation reached 0.23276 mm, with tooth deformation measuring 0.2216 mm and periodontal ligament deformation at 0.165 mm. The peak stress in the teeth was 63.298 MPa, localized at the junction between the tooth crown and root, while the maximum periodontal ligament stress was 0.41426 MPa. Condition ②: The maximum overall deformation was 0.23233 mm, tooth deformation 0.22133 mm, and periodontal ligament deformation 0.16472 mm. The maximum tooth stress recorded was 63.964 MPa at the crown-root interface, and the maximum periodontal ligament stress was 0.41566 MPa. Condition ③: The maximum overall deformation was 0.2321 mm, with tooth deformation of 0.22112 mm and periodontal ligament deformation of 0.16436 mm. The maximum tooth stress was 63.859 MPa, occurring at the crown-root contact, and the peak periodontal ligament stress was 0.41611 MPa. Condition ④: Overall maximum deformation reached 0.23235 mm, tooth deformation 0.22134 mm, and periodontal ligament deformation 0.16469 mm. Maximum tooth stress was 63.96 MPa at the crown-root interface, and the maximum stress of the periodontal ligament was 0.4158 MPa. Condition ⑤: The overall maximum deformation was 0.23197 mm, with tooth deformation of 0.22096 mm and periodontal ligament deformation of 0.16457 mm. The maximum tooth stress was 63.703 MPa at the crown-root junction, and the maximum periodontal ligament stress was 0.41634 MPa (**Figures 4**-**8**).

Trend of anterior tooth movement

The total displacement across all working conditions was approximately 0.23 mm, with minimal variation ranging from 0.23 to 0.23276 mm. Conditions ③ and ⑤ exhibited slightly lower total displacements compared to the

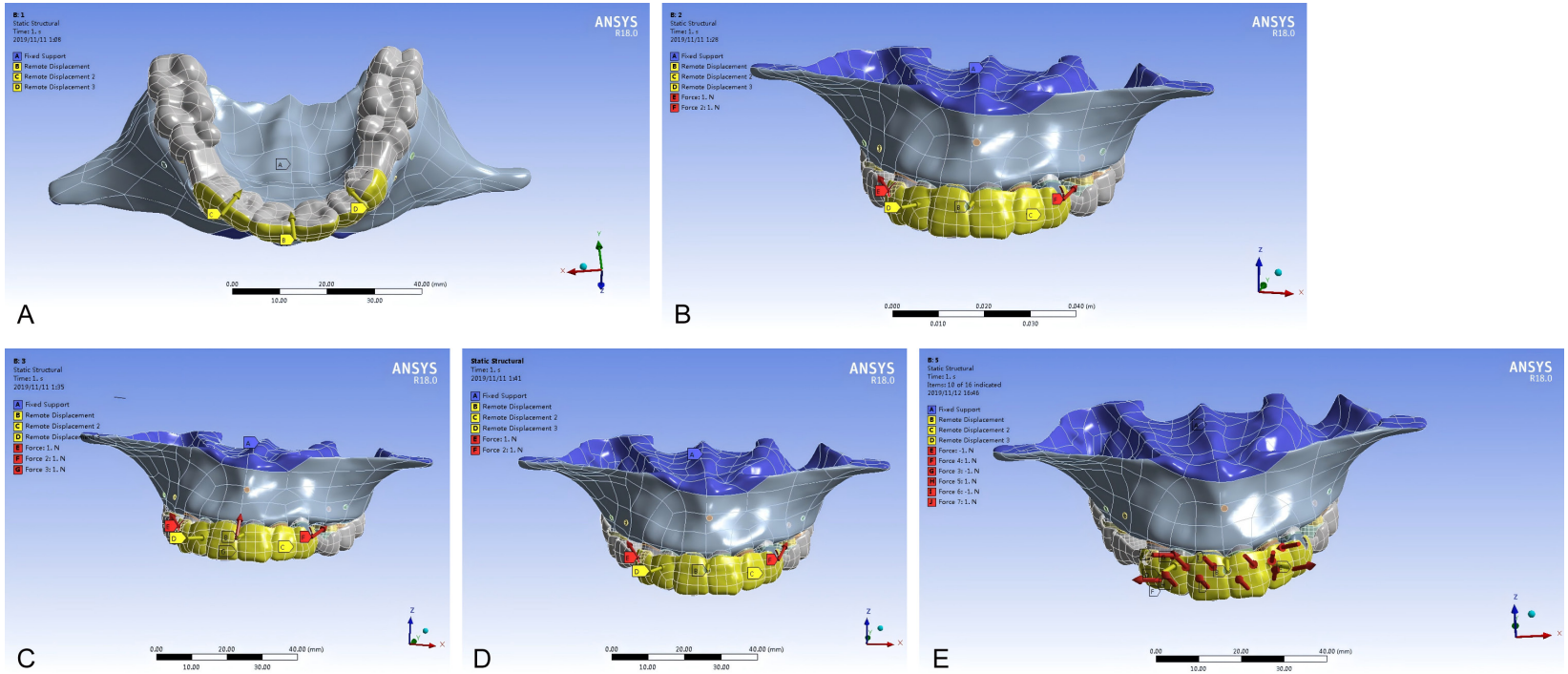

Figure 3. Three-dimensional finite element models of the anterior teeth retraction with the invisible orthodontic appliance under operating conditions ① through ⑤. A: Anterior teeth retraction with a 0.25 mm displacement load; B: 0.25 mm displacement load combined with a 1 N tensile force applied bilaterally; C: 0.25 mm displacement load with three 1 N force applications; D: 0.25 mm displacement load; E: 0.25 mm displacement load combined with 1 N loads applied to the upper and lower aspects of 6 cusp groups.

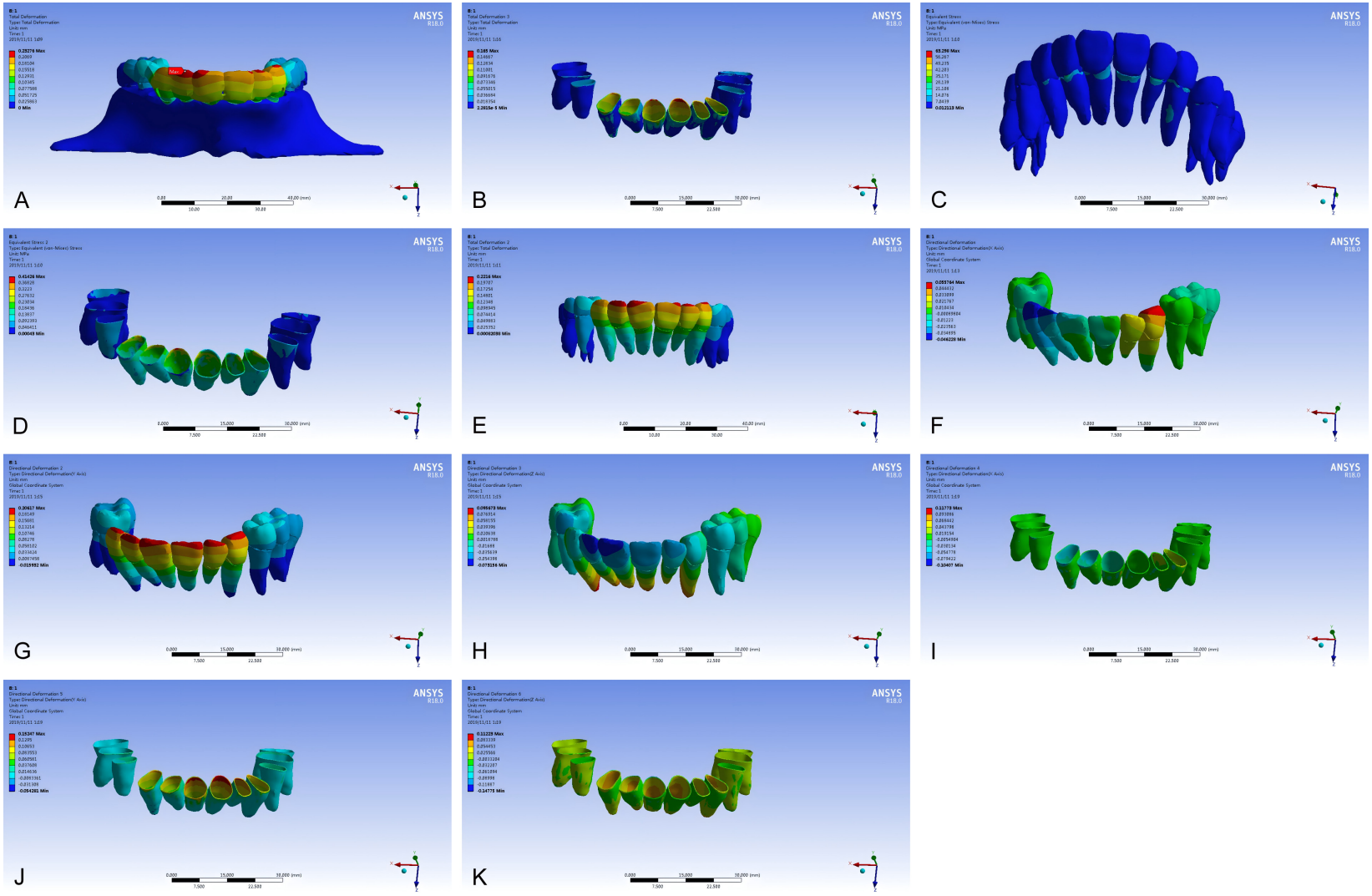

Figure 4. Cloud maps illustrating anterior teeth movement under working condition ①. A: Overall displacement; B: Periodontal ligament total deformation; C: Stress distribution at the coronal-radicular junction; D: Periodontal ligament stress distribution; E: Deformation of tooth crown and root; F: Coronal-radicular junction deformation in the X axis; G: Coronal-radicular junction deformation in the Y axis; H: Coronal-radicular junction deformation in the Z axis; I: Periodontal ligament deformation in the X axis; J: Periodontal ligament deformation in the Y axis; K: Periodontal ligament deformation in the Z axis.

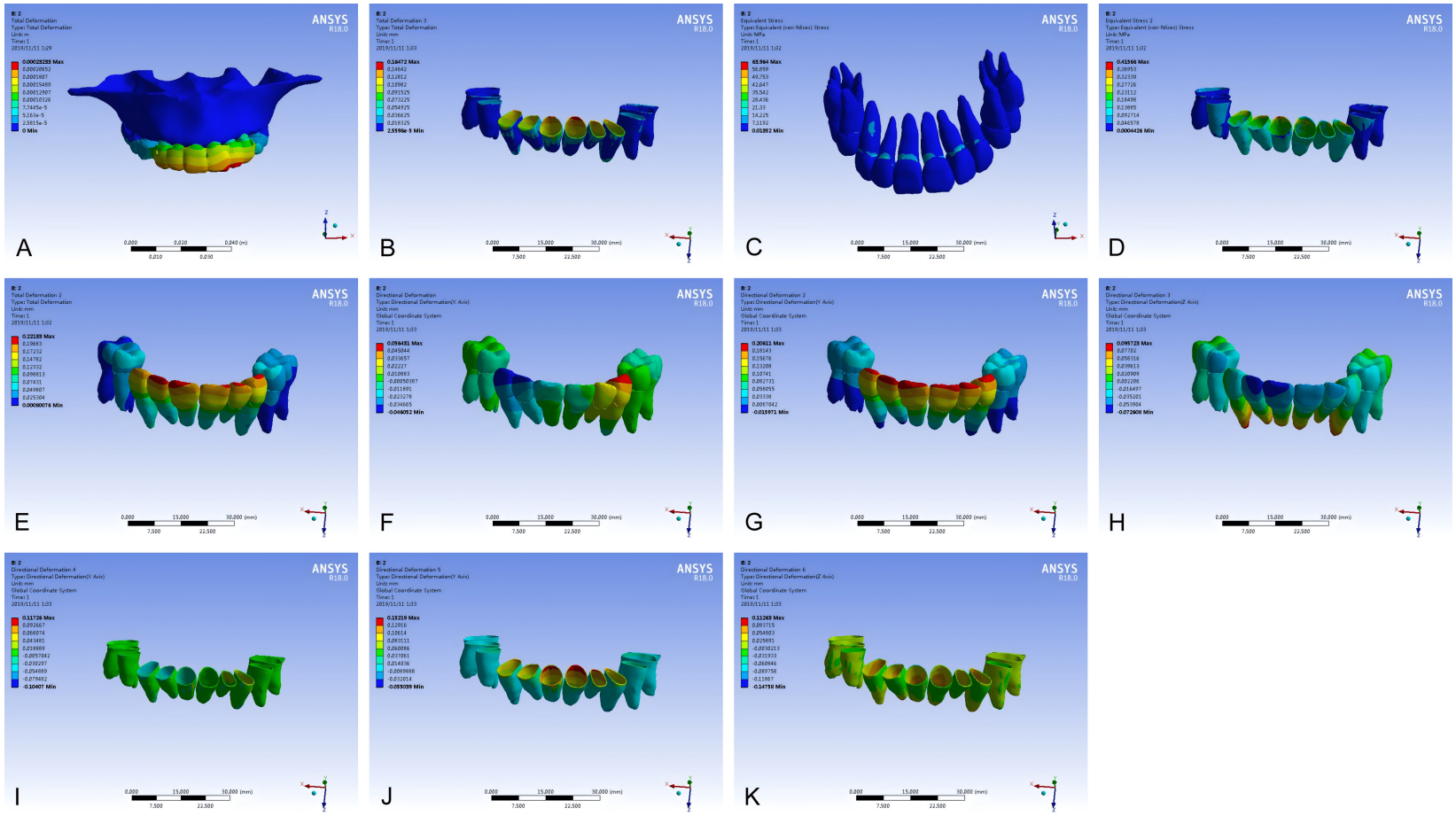

Figure 5. Cloud map illustrating anterior teeth movement under working condition ②. A: Overall displacement; B: Total deformation of the periodontal ligament; C: Stress distribution at the coronal-radicular junction; D: Stress distribution within the periodontal ligament; E: Deformation of tooth crown and root; F: Coronal-radicular junction deformation along the X axis; G: Coronal-radicular junction deformation along the Y axis; H: Coronal-radicular junction deformation along the Z axis; I: Periodontal ligament deformation along the X axis; J: Periodontal ligament deformation along the Y axis; K: Periodontal ligament deformation along the Z axis.

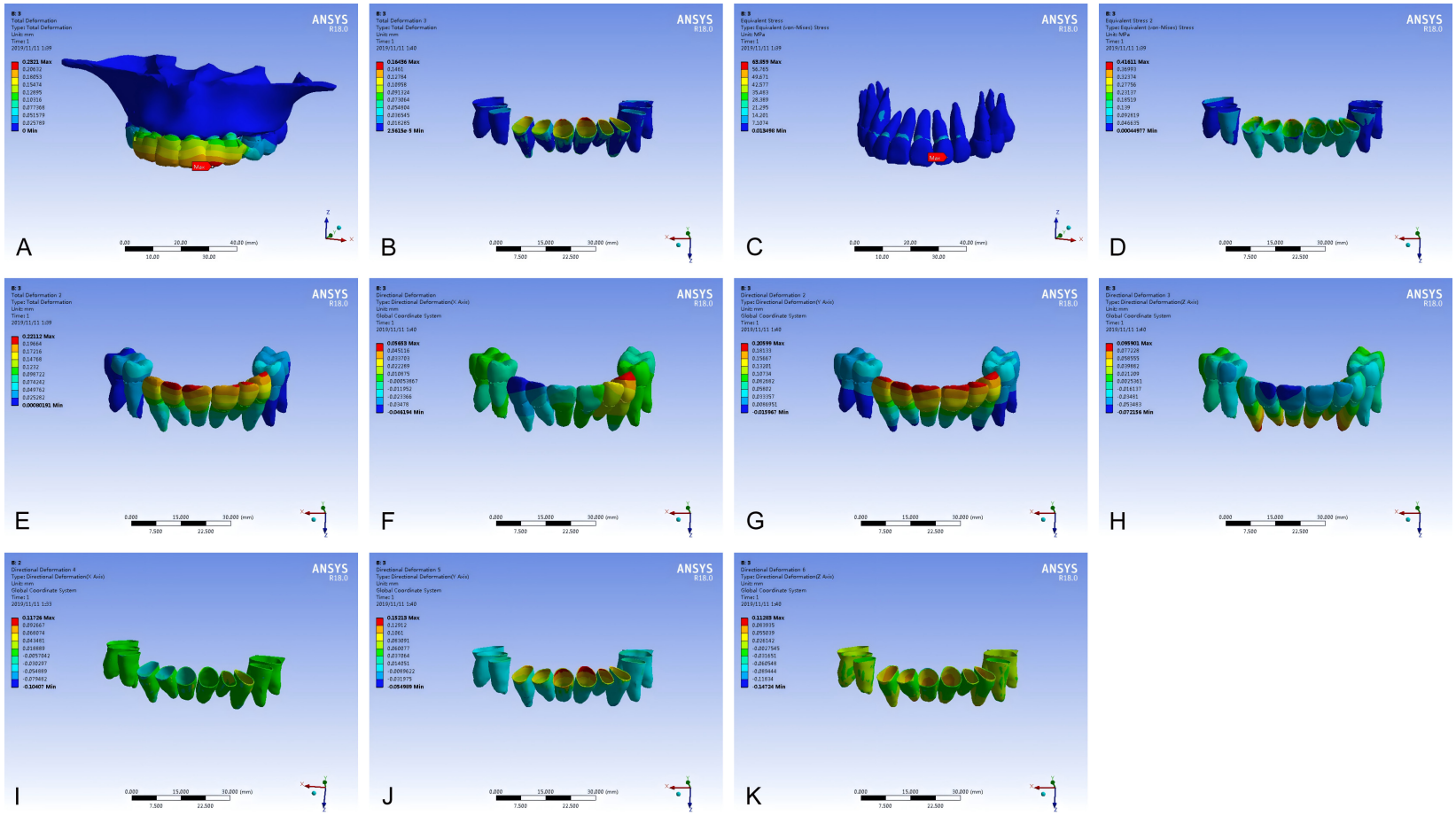

Figure 6. Cloud map illustrating anterior teeth movement under working condition ③. A: Overall displacement; B: Total deformation of the periodontal ligament; C: Stress distribution at the coronal-radicular junction; D: Stress distribution within the periodontal ligament; E: Deformation of the tooth crown and root; F: Coronal-radicular junction deformation along the X axis; G: Coronal-radicular junction deformation along the Y axis; H: Coronal-radicular junction deformation along the Z axis; I: Periodontal ligament deformation along the X axis; J: Periodontal ligament deformation along the Y axis; K: Periodontal ligament deformation along the Z axis.

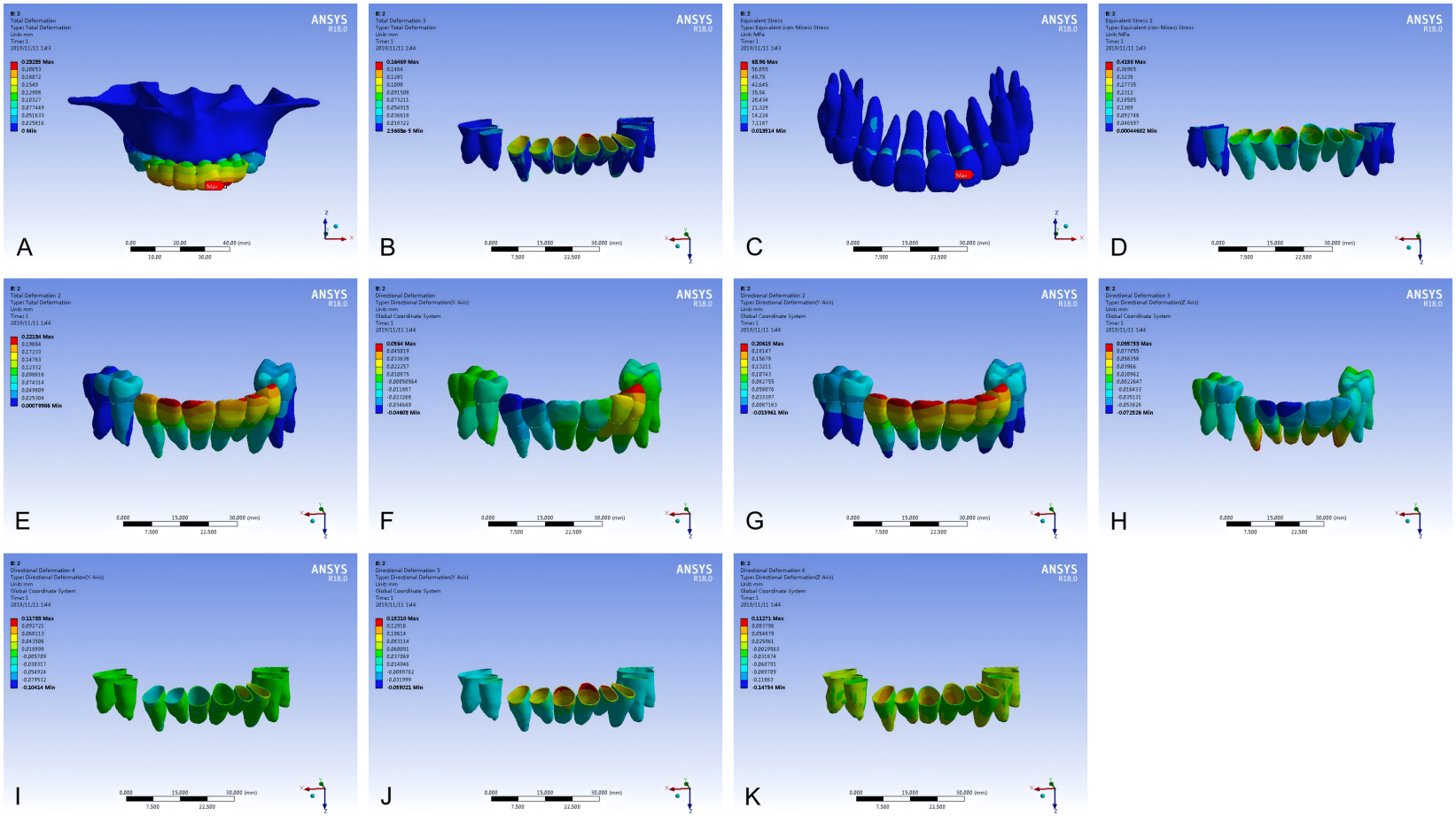

Figure 7. Cloud map illustrating anterior teeth movement under working condition ④. A: Overall displacement; B: Total deformation of the periodontal ligament; C: Stress distribution at the coronal-radicular junction; D: Stress distribution within the periodontal ligament; E: Deformation of the tooth crown and tooth root; F: Coronal-radicular junction deformation along the X axis; G: Coronal-radicular junction deformation along the Y axis; H: Coronal-radicular junction deformation along the Z axis; I: Periodontal ligament deformation along the X axis; J: Periodontal ligament deformation along the Y axis; K: Periodontal ligament deformation along the Z axis.

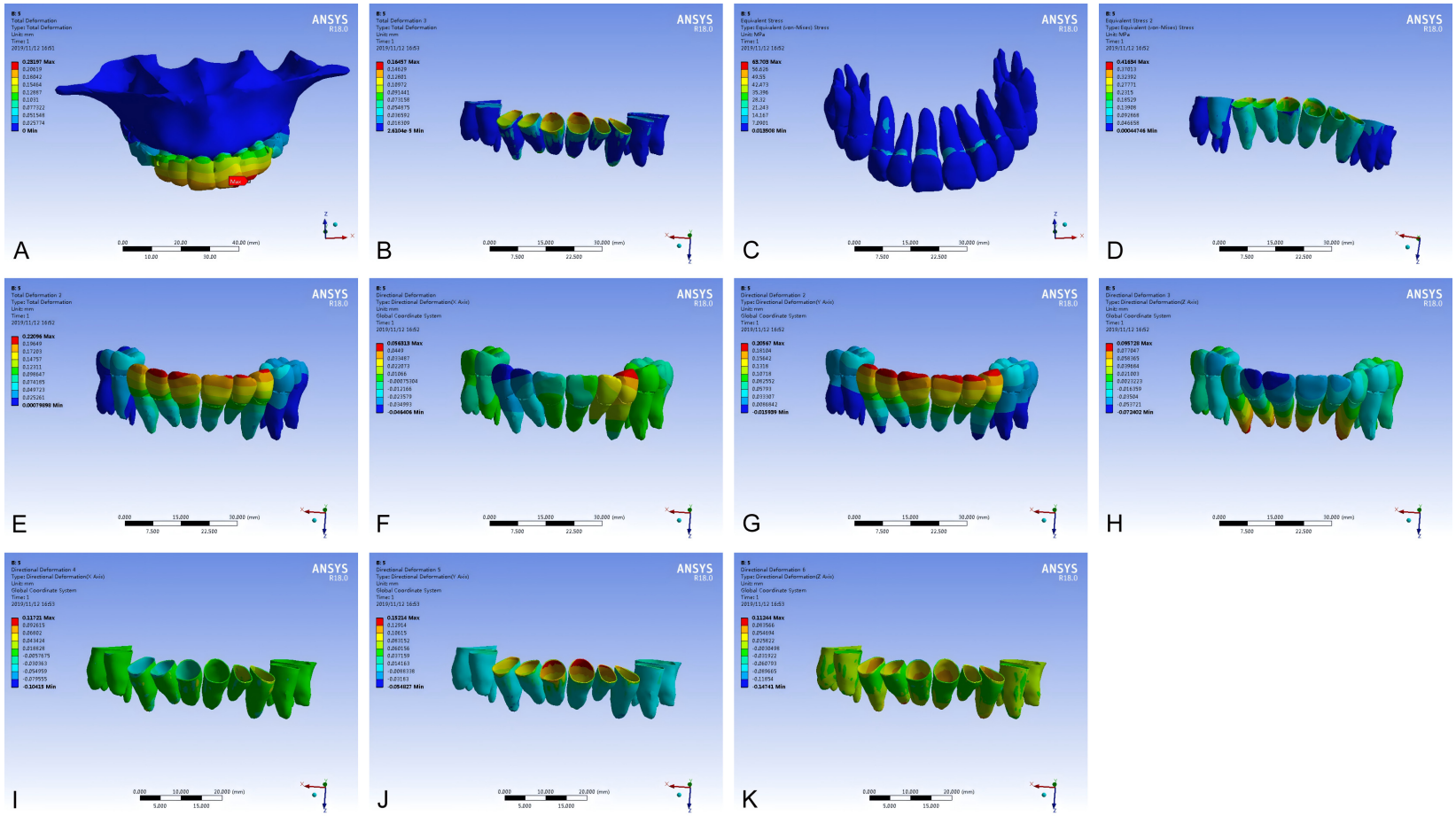

Figure 8. Cloud map illustrating anterior teeth movement under working condition ⑤. A: Overall displacement; B: Total deformation of the periodontal ligament; C: Stress distribution at the coronal-radicular junction; D: Stress distribution within the periodontal ligament; E: Deformation of the tooth crown and body; F: Coronal-radicular junction deformation along the X axis; G: Coronal-radicular junction deformation along the Y axis; H: Coronal-radicular junction deformation along the Z axis; I: Periodontal ligament deformation along the X axis; J: Periodontal ligament deformation along the Y axis; K: Periodontal ligament deformation along the Z axis.

other working conditions, though these differences were not significant. Stress values in the tooth crown and root ranged from 63.30 to 63.96 MPa. Conditions ② and ④ showed marginally higher stresses, while condition ⑤ demonstrated a slight reduction in stress (63.70 MPa), likely attributable to the application of root control technology. Periodontal ligament stress gradually increased from 0.41 MPa in condition ① to 0.42 MPa in condition ⑤, with the overall increase being limited. Displacement along the Y direction (labio-lingual direction) was predominant, measuring approximately 0.205-0.206 mm, while displacements along the x direction (mesio-distal) and Z direction (vertical) were comparatively smaller, around 0.055-0.056 mm and 0.095-0.096 mm, respectively. Although the differences in displacement between groups were minimal (0.001 mm), the stress reduction observed in condition ⑤ (0.26 MPa decrease, from 63.70 to 63.96 MPa) may help reduce the risk of cementum micro-injury, thus bearing potential clinical significance (**Table 2** and **Figure 9**).

Discussion

The fundamental principle of invisible orthodontic appliances is the generation of orthodontic force through the elastic deformation of the appliance itself. This force is transmitted to the teeth by close adaptation to the tooth surface, promoting tooth movement within the alveolar bone and thereby achieving alignment correction and occlusal improvement [6]. Invisible aligners are fabricated from high-molecular-weight materials with good elasticity and biocompatibility, such as thermoplastic polyurethane (TPU). These materials can undergo reversible elastic deformation under applied force. When the aligner is fitted onto the teeth, the discrepancy between its original shape and the current tooth position creates a restoring force that continuously acts on the teeth, promoting movement. Under the influence of this orthodontic force, a series of complex biological reactions occur within the periodontal tissues [7]. The periodontal ligament, serving as a critical connective structure between the tooth and alveolar bone, responds by activating resident cells that release various cytokines and enzymes, initiating remodeling processes. On the pressure side, osteoclastic activity increases, resulting in alveolar bone resorption. Conversely, on the tension side, osteoblastic activity is enhanced, promoting new bone formation. This coordinated bone resorption and deposition process enables the teeth to move slowly and in an orderly manner within the alveolar bone until the desired orthodontic position is achieved [8, 9].

Retraction of anterior teeth is a common and critical objective in orthodontic treatment, especially for patients with malocclusion such as maxillary protrusion and dentition crowding. This procedure effectively improves both facial aesthetics and occlusal function. However, during anterior tooth retraction with clear aligners, the mode of force transmission and the material properties differ significantly from those of traditional appliances, resulting in more complex tooth movement patterns and force dynamics. This complexity often leads to unwanted tooth tipping, which can exacerbate anterior deep bite and posterior open bite, ultimately compromising treatment effect and long-term stability [10, 11]. In clinical practice, clear aligners combined with micro-implant anchorage are often used to correct maxillary protrusion cases requiring tooth extraction, with generally favorable effects. However, the specific biomechanical mechanism remains poorly understood. Current stress application strategies are largely based on clinical experience rather than on specific biomechanical evidence. Variations in force magnitude, direction, point of application, as well as the aligner's thickness and elastic modulus, can significantly influence tooth movement and periodontal stress distribution during anterior teeth retraction [12]. Therefore, further investigation into these biomechanical effects is essential to optimize clear aligner treatment design, enhance therapeutic efficacy, and reduce complications.

In this study, five working conditions were established to comprehensively explore the biomechanical characteristics of upper anterior teeth retraction using clear aligners. Each condition was carefully designed to reflect realistic clinical scenarios. By simulating various methods and magnitudes of orthodontic force application, this study provides a rigorous and evidence-based theoretical basis for the optimization of clinical clear aligner treatment plans. The results showed that, across all working

Table 2. Displacement and stress measurements of the maxillary anterior tooth under different working conditions, including total displacement, stress at the coronal-radicular junction, periodontal ligament stress, crown and root displacement, as well as XYZ directional displacements of both the crown/root and periodontal ligament

Working Condition	Total displacement (mm)	Stress at the coronal-radicular junction (MPa)	Periodontal ligament stress (MPa)	Crown and dental position shift (mm)	Tooth crown and tooth body X displacement (mm)	Tooth crown and tooth body Y displacement (mm)	Tooth crown and tooth body Z displacement (mm)	Periodontal ligament displacement (mm)	Periodontal ligament X displacement (mm)	Periodontal ligament Y displacement (mm)	Periodontal ligament Z displacement (mm)
Working Condition 1	0.23	63.30	0.41	0.22	0.06	0.21	0.10	0.17	0.12	0.15	0.15
Working Condition 2	0.23	63.96	0.42	0.22	0.06	0.21	0.10	0.16	0.12	0.15	0.15
Working Condition 3	0.23	63.86	0.42	0.22	0.06	0.21	0.10	0.16	0.12	0.15	0.15
Working Condition 4	0.23	63.96	0.42	0.22	0.06	0.21	0.10	0.16	0.12	0.15	0.15
Working Condition 5	0.23	63.70	0.42	0.22	0.06	0.21	0.10	0.16	0.12	0.15	0.15

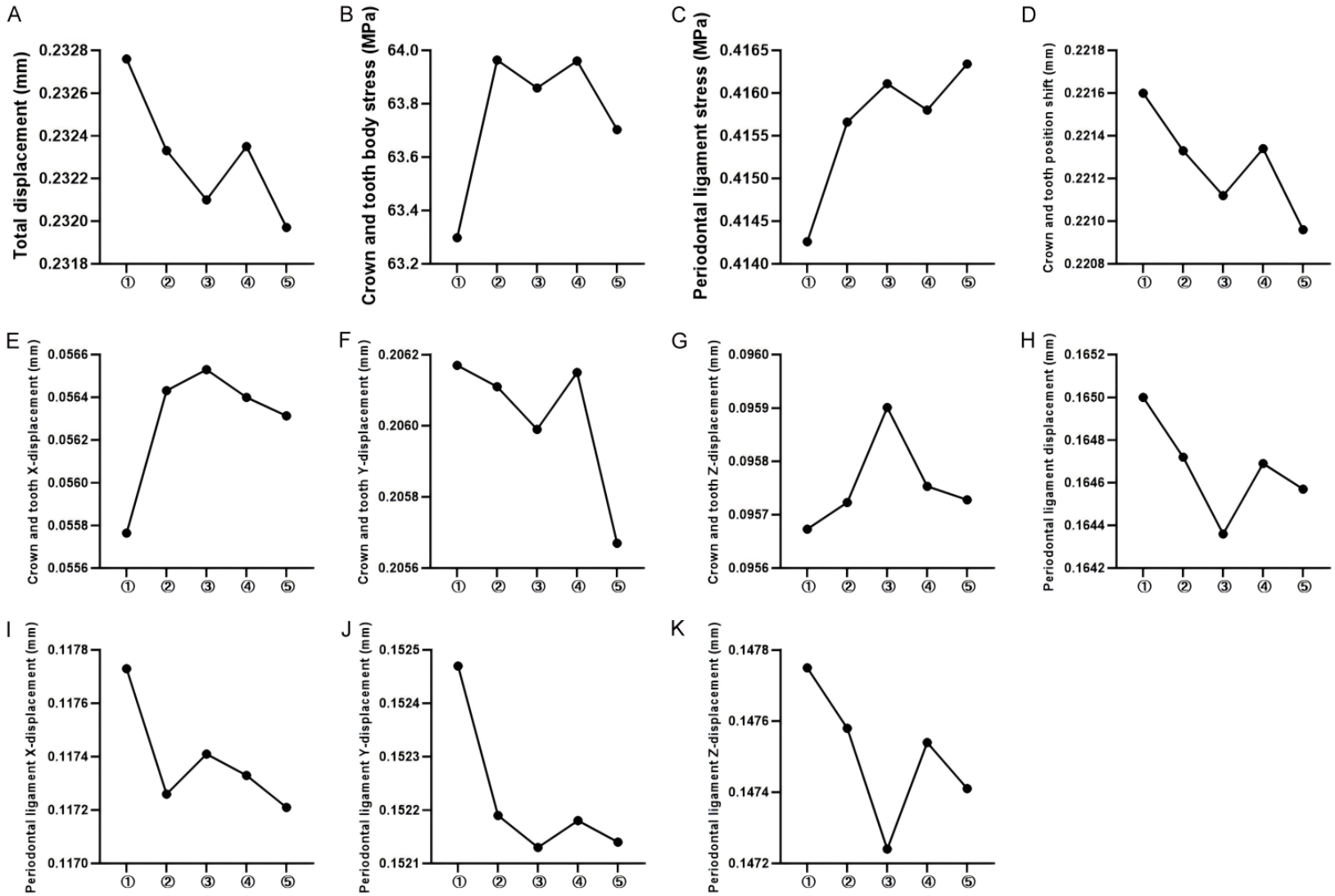

Figure 9. Shows the changes of stress and displacement under different working conditions. A: Comparison of total displacement under different working conditions; B: Stress distribution at the crown and tooth body; C: Stress distribution within the periodontal ligament; D: Comparison of crown and tooth positional shifts; E: Comparison of X-axis displacement of the crown and tooth body; F: Comparison of Y-axis displacement of the crown and tooth body; G: Comparison of Z-axis displacement of the crown and tooth body; H: Comparison of periodontal ligament displacement; I: Comparison of periodontal ligament displacement along the X-axis; J: Comparison of periodontal ligament displacement along the Y-axis; K: Comparison of periodontal ligament displacement along the Z-axis.

conditions, the maximum stress consistently occurred at the interface between the crown and the tooth body. This finding indicates that this region experiences heightened mechanical load during clear align treatment and represents a biomechanical vulnerability within the tooth structure [13]. The interface between the dental crown and the tooth body is a critical structural junction, where orthodontic forces transmitted through the crown lead to localized stress concentration. Prolonged exposure to excessive stress in this area may predispose the tooth to structural damage, including fractures and related complications [14, 15]. Under working condition ①, the maximum stress of the teeth was 63.298 MPa. This value increased to 63.964 MPa in condition ②, followed by 63.859 MPa in condition ③, 63.96 MPa in condition ④, and 63.703 MPa in condition ⑤. The variation in stress magnitudes across different working conditions reflects the significant influence that the mode and magnitude of applied orthodontic forces have on the stress distribution within the teeth. Specifically, when auxiliary forces from micro-implant screws are introduced, as seen in conditions ② to ④, the overall stress on the teeth increases. This is attributable to the extra complexity of force transmission, with the interface between the crown and the tooth body serving as the primary zone for force transfer and corresponding stress concentration [16, 17]. Regarding the periodontal ligament, the maximum stress distribution also varied among different conditions, though the maximum stress value was relatively low. In condition ①, the maximum periodontal ligament stress was 0.41426 MPa, which rose incrementally to 0.41566 MPa in condition ②, 0.41611 MPa in condition ③, 0.4158 MPa in condition ④, and 0.41634 MPa in condition ⑤. This gradual increase in periodontal ligament stress correlates with the escalation and alteration of applied orthodontic forces, indicating that the periodontal ligament consistently endures a certain level of mechanical load during clear aligner therapy. However, excessive stress may negatively affect periodontal health, potentially leading to periodontal ligament damage and alveolar bone resorption [18, 19]. The maximum stress of the periodontal ligament under conditions ① and ② shows an upward trend, indicating that the augmentation of tensile forces on both sides leads to a corresponding rise in the stress borne by the periodontal ligament. This suggests a heightened mechanical response of the periodontal ligament during the orthodontic process. In condition ③, an additional 1 N force is applied between the maxillary central incisors based on condition ②, resulting in a further reduction in overall deformation. Correspondingly, the maximum stress of the tooth crown and body also changes, indicating that this supplementary force uniquely influences the mechanical response of the teeth, changing both the deformation trend and the regions of stress concentration. In terms of displacement, notable differences were observed in the XYZ directional movements of both teeth and periodontal ligament across the working conditions. Specifically, under condition ①, tooth deformation along the XYZ directions measured 0.055764 mm, 0.20617 mm, and 0.095673 mm, respectively. The corresponding periodontal ligament deformation was 0.11773 mm, 0.15247 mm and 0.14775 mm, respectively. Under condition ②, tooth deformation in the XYZ directions was 0.056431 mm, 0.20611 mm, and 0.095723 mm, respectively, while periodontal ligament deformation measured 0.11726 mm, 0.15219 mm and 0.14758 mm along the same axes. The displacements of teeth and periodontal ligament in different directions under different orthodontic conditions reflect the significant influence of both the magnitude and direction of applied orthodontic forces. When additional orthodontic forces are introduced at specific points, such as via micro-implant screws or other methods in working conditions ② through ⑤, the corresponding directional displacements of teeth and periodontal ligament alter accordingly. This highlights the critical role of the force application site and vector in determining tooth movement and periodontal ligament deformation [20].

Notably, this study, employing finite element analysis, was the first to demonstrate that the dynamic ridge technique can reduce the peak stress on the periodontal ligament by 0.02 MPa, providing a biomechanical rationale for clinical root-controlled tooth retraction. Future work should validate these findings through clinical randomized controlled trials (RCTs). Prospective studies could compare the clinical efficacy of working condition ⑤ against tradi-

tional retraction regimens, assessing root resorption levels and retraction efficiency after 3 months of treatment.

The findings of this study provide a biomechanical foundation to guide clinicians in selecting optimal clear aligner treatment strategies tailored to individual patient conditions. For cases with minimal difficulty in retracting the upper anterior teeth and low anchorage demands, the overall retraction approach represented by working condition ① may be appropriate. In contrast, for patients requiring stronger anchorage, such as those presenting with significant dental crowding or protrusion, alternative anchorage configurations and force application methods, as simulated in working conditions ② through ④, offer valuable options. For cases necessitating precise control over root position and angulation, the simulated power ridge model of root-controlled retraction provides critical clinical insight. Treatment planning should be personalized, taking into account factors including the severity of tooth deformity, periodontal health status, and root morphology. In patients with compromised periodontal health, excessive orthodontic forces should be avoided, favoring force distributions that minimize localized stress concentrations. Moreover, integrating advanced technologies such as 3D printing can facilitate customized appliance fabrication, better conforming to the patient's tooth morphology and treatment needs. Digital technology, including intraoral scanning and CBCT, should be used for real-time monitoring of tooth movement and periodontal tissue changes, enabling timely adjustments to the treatment plan.

This study was limited to a single adult patient with maxillary protrusion. The small sample size and lack of diversity in patient age and malocclusion types may restrict the generalizability of the results. Future research should include at least 30 patients with different malocclusion types-such as Angle's Class II Division 1 and dental crowding- to validate the universality of the observed stress patterns, ideally integrating CBCT-based dynamic monitoring. Subsequent studies should employ a multi-center, large-sample design, combined with 3D printing technology to construct personalized models. This approach would allow for a more comprehensive evaluation of how different microimplant placement sites (e.g., incisor region vs first premolar area) affect biomechanical stress distribution.

Conclusions

Based on the experimental data and related data analyses, the following conclusions were drawn: ① Regardless of the working condition, the maximum stress on the tooth consistently concentrates at the junction between the crown and the tooth body; ② The displacements of teeth and periodontal ligament along the X, Y and Z directions exhibit distinct patterns under different working conditions, highlighting the significant influence of different clear aligner force application modes on tooth and periodontal ligament movement. ③ For patients with mild crowding of the upper anterior teeth and good periodontal health, whole retraction of the upper anterior teeth-as modeled in condition ①-can serve as a reference for treatment planning. Conversely, for patients facing greater difficulty in anterior tooth retraction and requiring precise root control, the biomechanical insights from the power ridge technique demonstrated in condition ⑤ provide valuable guidance for developing tailored treatment plans.

Acknowledgements

This work was supported by the Hospital-level scientific Research of Hanzhong Central Hospital (Project No.: YK1903).

Disclosure of conflict of interest

The authors declare that the research was conducted in the absence of any commercial or financial relationships that could be construed as a potential conflict of interest.

Address correspondence to: Jing Xiong, Department of Stomatology, Hanzhong Central Hospital, Hanzhong 723000, Shaanxi, China. E-mail: 15619833031@163.com

References

[1] Inchingolo AM, Inchingolo AD, Carpentiere V, Del Vecchio G, Ferrante L, Di Noia A, Palermo A, Di Venere D, Dipalma G and Inchingolo F. Predictability of dental distalization with clear aligners: a systematic review. Bioengineering (Basel) 2023; 10: 1390.

[2] Yu X, Li G, Zheng Y, Gao J, Fu Y, Wang Q, Huang L, Pan X and Ding J. 'Invisible' orthodontics by

polymeric 'clear' aligners molded on 3D-printed personalized dental models. Regen Biomater 2022; 9: rbac007.
[3] Chen J, Zhu D, Zhao M, Cheng Z, Pan Y and Liu X. Three-dimensional finite element analysis of the optimal mechanical design for maximum inward movement of the anterior teeth with clear aligners. Sci Rep 2024; 14: 13203.
[4] Cheng Y, Liu X, Chen X, Li X, Fang S, Wang W, Ma Y and Jin Z. The three-dimensional displacement tendency of teeth depending on incisor torque compensation with clear aligners of different thicknesses in cases of extraction: a finite element study. BMC Oral Health 2022; 22: 499.
[5] Lin C, Hu H, Zhu J, Wu Y, Rong Q and Tang Z. Influence of sagittal root positions on the stress distribution around custom-made root-analogue implants: a three-dimensional finite element analysis. BMC Oral Health 2021; 21: 443.
[6] Narongdej P, Hassanpour M, Alterman N, Rawlins-Buchanan F and Barjasteh E. Advancements in clear aligner fabrication: a comprehensive review of direct-3D printing technologies. Polymers (Basel) 2024; 16: 371.
[7] Rodríguez Fernández JC, Pastor F, Mora JMB, Demiquels E, Espinar E and Gil J. Conformation effect on the mechanical and microbiological behavior of invisible orthodontic aligners. Materials (Basel) 2024; 17: 1360.
[8] Tania M, Veerasankar S, Ponniah H, Dhayananth LX, Preeti R and Missier MS. Comparison of patient satisfaction between invisible appliance and fixed orthodontic appliances - a systematic review. J Pharm Bioallied Sci 2024; 16: 1017-1021.
[9] Ahmed T, Padmanabhan S and Pottipalli Sathyanarayana H. Effects of varying attachment positions on palatal displacement of maxillary incisors with clear aligner therapy: a three-dimensional finite element analysis. J Orofac Orthop 2023; 84: 178-188.
[10] Sun ZT, Wang YC, Cui YM and Sun Y. Finite element analysis of maxillary anterior teeth retraction of posterior teeth with different alveolar bone absorption heights under orthodontic force. West Chi J Stomat 2019; 37: 265-269.
[11] Li ZX, Yuan LJ, Zheng XW, Liu L, Liu C and Fang B. Comparison of clear aligners and customized lingual appliance for bimaxillary dentoalveolar protrusion: a retrospective study. Shanghai Stomat 2023; 32: 480-484.
[12] Bai Y, Feng X, Liu DM, Li P and Feng YL. Three-dimensional finite element study on the overall adduction of anterior teeth using braceless invisible orthodontic appliances combined with micro-implant nails. J Pract Stomat 2019; 35: 71-76.
[13] Fan LM, Liu RX and Xu BH. Three-dimensional finite element study on the traction and adduction of anterior teeth with braceless invisible orthodontic appliances combined with micro-implant nails. J China-Japan Friend Hos 2022; 36: 152-155.
[14] Castroflorio T, Sedran A, Parrini S, Garino F, Reverdito M, Capuozzo R, Mutinelli S, Grybauskas S, Vaitiekūnas M and Deregibus A. Predictability of orthodontic tooth movement with aligners: effect of treatment design. Prog Orthod 2023; 24: 2.
[15] Maldonado Molina OA. Orthodontics and dental implants in the esthetic zone. J Clin Orthod 2023; 57: 411-417.
[16] Gao Y, Chen YH, Wang LC, Guo ZY, Liu L and Fu SM. Three-dimensional finite element study of anterior teeth retraction in different ways with lingual movable wing orthodontic appliances. J Pract Stomat 2023; 39: 192-197.
[17] Guo R, Lam XY, Zhang L, Li W and Lin Y. Biomechanical analysis of miniscrew-assisted molar distalization with clear aligners: a three-dimensional finite element study. Eur J Orthod 2024; 46: 77.
[18] Liao X, Cao R, Zhong J, Chen C and Pan S. Influence of implant distribution on the biomechanical behaviors of mandibular implant-retained overdentures: a three-dimensional finite element analysis. BMC Oral Health 2024; 24: 405.
[19] Jain A, Prasantha GS, Mathew S and Sabrish S. Analysis of stress in periodontium associated with orthodontic tooth movement: a three dimensional finite element analysis. Comput Methods Biomech Biomed Engin 2021; 24: 1841-1853.
[20] Mao B, Tian Y, Li J and Zhou Y. Expansion rebound deformation of clear aligners and its biomechanical influence: a three-dimensional morphologic analysis and finite element analysis study. Angle Orthod 2023; 93: 572-579.